CHIN. PHYS. LETT. Vol. 36, No. 12 (2019) 127601

High Resolution Microwave B-Field Imaging Using a Micrometer-Sized Diamond Sensor *

Wen-Hao He(和文豪)[1], Ming-Ming Dong(董明明)[1], Zhen-Zhong Hu(胡振忠)[1], Qi-Han Zhang(张琪涵)[2], Bo Yang(杨博)[1], Ying Liu(刘颖)[1], Xiao-Long Fan(范小龙)[2], Guan-Xiang Du(杜关祥)[1]**

[1]*College of Telecommunication & Information Engineering, Nanjing University of Posts and Telecommunications, Nanjing 210000*

[2]*School of Physical Science and Technology, Lanzhou University, Lanzhou 730000*

(Received 24 September 2019)

We propose a diamond-based micron-scale sensor and perform high-resolution B-field imaging of the near-field distribution of coplanar waveguides. The sensor consists of diamond crystals attached to the tip of a tapered fiber with a physical size on the order of submicron. The amplitude of the B-field component B is obtained by measuring the Rabi oscillation frequency. The result of Rabi sequence is fitted with a decayed sinusoidal. We apply the modulation-locking technique that demonstrates the vector-resolved field mapping of the micromachine coplanar waveguide structure (CPW). B-field line scan was performed on the CPW with a scan step size of 1.25 μm. To demonstrate vector resolved rf field sensing, a full field line scan acts (was performed) along four NV axes at a height of 50 μm above the device surface. The simulations are compared with the experimental results by vector-resolved measurement. This technique allows the measurement of weak microwave signals with a minimum resolvable modulation depth of 20 ppm. The sensor will have great interest in micron-scale resolved microwave B-field measurements, such as electromagnetic compatibility testing of microwave integrated circuits and characterization of integrated microwave components.

PACS: 76.30.Mi, 76.70.Hb DOI: 10.1088/0256-307X/36/12/127601

High resolution imaging of microwave near-field has long challenged although a variety of measurement techniques have been developed, such as miniature inductive loop,[1,2] electro-optic and magneto-optic probe.[3–5] These techniques are either bulky or having inevitable electromagnetic coupling effect, which are not satisfactory for integrated circuit electromagnetic compatibility testing. In integrated circuit electromagnetic compatibility testing, microwave function units are densely arranged on a millimeter-scale chip with characteristic size of a few micrometers. The diagnosis and location of signal cross-talks need to observe the local field distribution with micron resolution in electromagnetic compatibility testing. In the meantime, novel techniques such as spintronic microwave detector,[6] atomic microwave imager[7] and diamond spin sensor[8] have been demonstrated, but so far satisfactory near field sensing techniques remain an open issue. In this Letter, we propose a fiber-based diamond rf B-field sensor with a size of about 10 μm, which is minimally invasive and robust in operation. We report a fiber-based rf field probe and demonstrate sub-100 micrometer spatial resolution in a small helical antenna.[9] In Ref. [9], we also proposed a pulsed modulation technique, which can measure very weak fluorescence (FL) sideband signals with a noise floor of about 100 nV. This noise level corresponds to a minimum resolvable microwave modulation depth of 20 ppm, which is defined by the FL change upon pulsed microwave driving at resonance. In this work, we develop a procedure to fix sub-10 micrometer diamond crystal on fiber tip under a microscope with a controlled way and demonstrate this micro probe on a micro-fabricated coplanar waveguide structure (CPW).

The microwave B-field probe is a diamond crystal containing nitrogen vacancy (NV) center, a spin-dependent photo luminescent atomic defect in diamond crystal with spin coherence under ambient conditions. Electron irradiated HPHT diamond microcrystals have enriched NV centers. We developed a microscope system to prepare the fiber-diamond probe in a well-controlled way. The procedure is experimentally challenging and handy to operate should be assisted with a homemade dark-field microscope. The tapered fiber is mounted on a three-axis manual translation stage, which is brought near the surface of a glass slide, coated with well dispersed diamond crystals, with size ranging from a few to tens of micrometers. The fiber tip is prepared by stretching the fiber under flame heating to enhance the excitation and collection efficiency. The distance of the fiber tip from the glass top surface is estimated by the separation of the fiber tip and its inverted mirror image. To locate a desired crystal, the green light is guided to the fiber tip, which excites the diamond crystal, and FL emitted by the diamond is collected. The intensity of FL is used as a rough estimation of the crystal size. Note that the fiber tip is dipped with a tiny drop of UV curable glue before picking up the desired diamond crystal, which is the last step of curing under UV LED. A stable FL intensity is very critical in this procedure for

*Support by the Jiangsu Distinguished Professor Program under Grant No RK002STP15001, and the NJUPT Principal Distinguished Professor Program under Grant No NY214136.

**Corresponding author. Email: duguanxiang@njupt.edu.cn

© 2019 Chinese Physical Society and IOP Publishing Ltd

fine moving of fiber, which is accomplished by gating periodically the excitation laser. The gating shifts low frequency intensity noise of laser to higher frequency, where the noise power is much weaker and the fluorescence readout is stabilized.

A negatively charged NV center (hereafter noted as the NV center) is an excellent nanoscale quantum sensor for magnetic-electric field and temperature sensing. The ground state of the NV center is spin triplet with magnetic sublevels $m_s = 0$ and $m_s = \pm 1$. Magnetically allowed dipole transition can be driven between $m_s = 0$ and $m_s = \pm 1$, according to quantum state symmetry. These two transitions are sensitive to the circular polarization components in the plane normal to the NV axis. The degeneracy of the $m_s = \pm 1$ state can be lifted by applying an external static magnetic field. Since NV centers have four equivalent orientations in diamond crystal, a total of eight peaks are observed in the optically detected magnetic resonance (ODMR) spectrum.[10] The FL contrast, which is the ratio of FL change upon microwave driving to that without microwave driving, is ∼30% for a single NV center. However, because there are four NV center orientations and a total of eight allowed transitions, the contrast drops to ∼4% for each transition in NV ensemble, which is further reduced due to the FL from NV^0.[11] On the other hand, the excitation green laser intensity noise is on the order of 0.5%, which sets a limit on the minimum observable contrast without averaged measurements.

To increase the signal-to-noise ratio, modulation of microwave, either in amplitude or in frequency is a powerful technique and has been well established in continuous-wave ODMR.[12,13] Implementing this modulation technique in pulsed ODMR is not yet obvious, but applicable. In addition to pulsed ODMR, where microwave and laser are switched by synchronized pulse sequence, a global modulation with a relatively low frequency f_m (in this work $f_m = 909.09$ Hz) is further applied to the microwave signal source. This global modulation generates a sideband of the FL signal at the microwave resonance that is otherwise absent at off-resonance. This frequency domain measurement is a complementary to the time domain measurement.[14] It can be seen from the comparison data (not shown) that the advantage associated with frequency measurement is that the noise can be better suppressed, and the noise can be reduced from dc or low frequency laser intensity noise to high frequency, which can significantly reduce the noise power. The high dynamic range and sensitivity to weak electric signal in most spectrum equipment's measurement such as signal analyzer and lock-in amplifier is also an obvious advantage.

Figure 1 is the sketch of the system. The laser emits 532 nm continuous laser, which is switched by an acousto-optic modulator (AOM), and the intensity is adjusted by a half wave plate and polarized beam splitter (PBS). The pulsed laser is reflected to the objective lens with long working distance by a dichroic mirror, which is coupled to the optical fiber. The other end of the optical fiber is connected with diamond crystal. The device under test (DUT) is fixed on a motorized stage. The fluorescence (FL) emitted by the diamond is collected by the objective lens, transmitted through the dichroic lens, and collected by a short working distance objective lens to the active area of the avalanche photodiode (APD). A long-pass filter is installed on the APD for filter out the green laser. The diameter of the diamond crystal is measured to be 9.5 μm under a calibrated home build FL microscope.

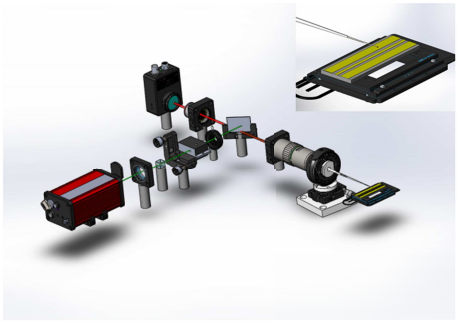

Fig. 1. System sketch, the field sensor is a diamond crystal attached to the fiber tip, which is excited by a pulsed green laser and its FL is collected and detected by an APD.

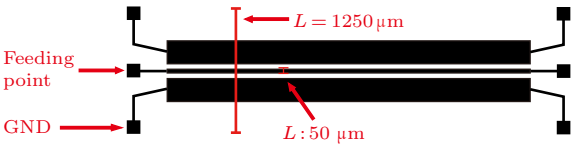

Fig. 2. Photograph of the micro-fabricated waveguide. The center conductor and the gap are both 50 μm in width.

Figure 2 shows the photograph of the miniature coplanar waveguide on a gadolinium gallium garnet (GGG) single crystal substrate. The gap between the central conductor Pt strip and grounding strip is also 50 μm where the width of the Pt strip is also 50 μm. Note that only one ground plane is electrically connected and the other is floating, which has been used to study the ferromagnetic resonance of magnetic thin films before.[15] The detailed description of the field probing system can be found elsewhere.[9]

Pulsed ODMR sequence is composed of an interlaced laser and MW pulse, with laser pulse duration of 500 ns, which both polarizes and readouts the spin state.[16] With laser turned off, a resonant microwave pulse drives the spin state evolution between $m_s = 0$ and $m_s = \pm 1$ in the closed Rabi cycle on the spin Bloch sphere.[17,18] Besides this well-established pulse sequence, the MW is further amplitude modulated at the signal source at a relatively low frequency $f_m = 909.09$ Hz. Resonant microwave driving thus results in a sideband signal of the fluorescence carrier, with a frequency shift of f_m. A typical ODMR spectrum is shown in Fig. 3(a). A permanent magnet splits the degeneracy of the $m_s = \pm 1$ state along the four NV axes, thereby observing eight peaks. Each peak measures a transverse circular polarization component along one of the NV axes, which forms the basis of vec-

torial reconstruction of field vector. The amplitude of the B-field component B is obtained by measuring the Rabi oscillation frequency Ω via the relationship of $\Omega = \gamma B$, where γ is the electron spin gyromagnetic ratio. The result of Rabi sequence is fitted with a decayed sinusoidal, as shown in Fig. 3(b).

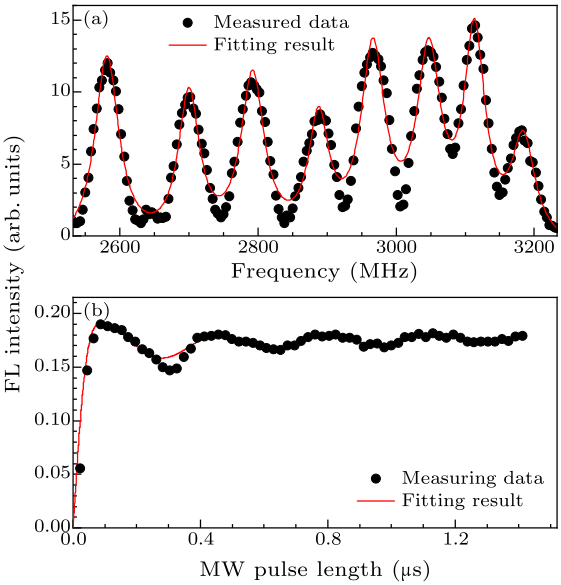

Fig. 3. Characterization of the rf field sensor. (a) Pulsed ODMR spectrum showing eight different peaks of all the four NV axes. (b) Rabi oscillations of the diamond NV center.

Figure 4 reveals the B-field line scan across the CPW with a scanning step size of 1.25 μm. The field distribution is simulated by HFSS.[19,20] The simulation was performed on a plane 5 μm from the surface of the CPW. The spatial resolution determined by the size of the crystal can be possibly extended to submicron or even nano-scale.[21] According to the evaluation of a wide field diamond microscope,[8,22] the scanning probe has a small overall size (minimized invasiveness) and can be brought into complex geometries (for example, through holes in the PCB). To demonstrate vector-resolved rf field sensing, a full set of field line scan was performed along the four NV axes at a height of 50 μm above the device surface. Each of the four NV axes measures the transverse circular polarization of rf field projected in the plane normal to the NV axis. As shown in Fig. 5(a), the line profiles for the four crystal orientations are obviously different. A further quantitative comparison of the line profiles with HFSS simulations will require knowledge of the crystal orientation of the diamond particles in laboratory frame. Instead, we wrote an MATLAB code to analytically simulate the field line scan profiles along four different projections, indexed by 1 to 4 in Fig. 5(b). We consider two infinitely long element currents along the z-axis confined at the edge of the center conductor with spacing of 50 μm, which is a good approximation of the actual current distribution in the center conductor due to skin effect of microwave current.[22] The four projections with index 1–4 axes are oriented in the xy-plane and form angles of 170°, 30°, 95° and 150° with respect to the x-axis, respectively. Because one of the ground plane of the coplanar waveguide is not electrically wired, the current on both edges of the conductor is unbalanced. In this simulation, we set the current ratio to 7:3 and find a good agreement between the measured and simulated field line profiles. It should be noted that this simulation is a rather simple illustration of the vector-resolved measurement, the four projection axes are chosen arbitrarily in the plane normal to the current flow direction.

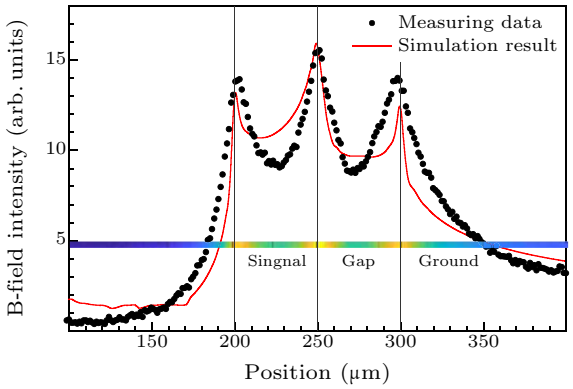

Fig. 4. Line scan of a coplanar waveguide and its HFSS simulation results.

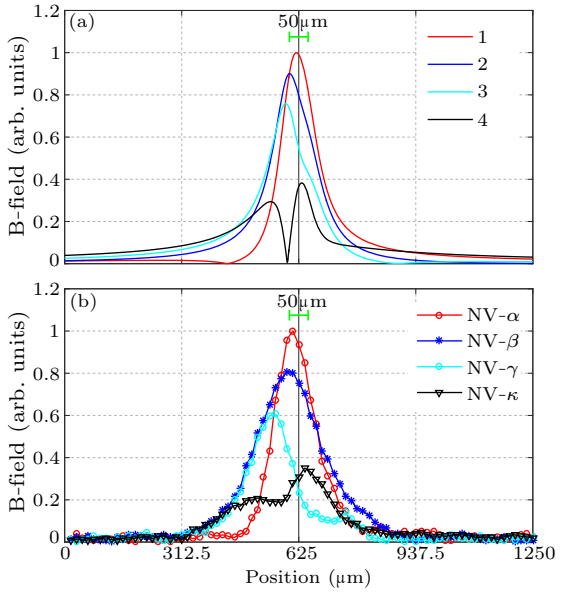

Fig. 5. Vector-resolved microwave magnetic field. (a) MATLAB simulation of the field distribution projected along four different orientations. (b) Measured field vector components along four NV axes.

In conclusion, we have developed a sub-10 micrometer rf field probing system in fiber format. The sensing element is a micro-sized diamond crystal containing NV centers. Experimental procedures of preparing the micro-sized probe is established under a microscope. Modulated lock-in technique is applied to allow us to measure weak microwave signals with a demonstrated minimum resolvable modulation depth

of 20 ppm. We demonstrate vector resolved field mapping of a micro-fabricated CPW structure and write an MATLAB code to reproduce the observed field line profiles.

G. X. Du thanks careful reading of the manuscript and English polishing by Dr. Caihua Wan at IOP, CAS.

References

[1] Baker-Jarvis J, Janezic M D, Domich P D and Geyer R G 1994 *IEEE Trans. Instrum. Meas.* **43** 711
[2] Peterson P Y, Gallimore A D and Haas J M 2002 *Phys. Plasmas* **9** 4354
[3] Song H J, Shimizu N and Nagatsuma T 2007 *Opt. Express* **15** 14901
[4] Iwanami M, Hoshino S, Kishi M and Tsuchiya M 2004 *Jpn. J. Appl. Phys.* **43** 2288
[5] Yamazaki E, Park H, Wakana S, Kishi M and Tsuchiya M 2002 *International Topical Meeting on Microwave Photonics* (Awaji, Japan 5–8 November 2002) (unpublished)
[6] Wang C, Cui Y T, Katine J A, Buhrman R A and Ralph D C 2011 *Nat. Phys.* **7** 496
[7] Xia H, Baranga A B A, Hoffman D and Romalis M V 2006 *Appl. Phys. Lett.* **89** 211104
[8] Yang B, Dong Y, Hu Z Z, Liu G Q, Wang Y J and Du G X 2018 *IEEE Trans. Microwave Theory Tech.* **66** 2276
[9] Dong M M, Hu Z Z, Liu Y, Yang B, Wang Y J and Du G X 2018 *Appl. Phys. Lett.* **113** 131105
[10] Neumann P, Kolesov R, Jacques V, Beck J, Tisler J, Batalov A, Rogers L, Manson N B, Balasubramanian G, Jelezko F and Wrachtrup J 2009 *New J. Phys.* **11** 013017
[11] Rondin L, Tetienne J P, Hingant T, Roch J F, Maletinsky P and Jacques V 2014 *Rep. Prog. Phys.* **77** 056503
[12] Horowitz V R, Aleman B J, Christle D J, Clel, A N and Awschalom D D 2012 *Proc. Natl. Acad. Sci. USA* **109** 13493
[13] Braun D and Libchaber A 2002 *Opt. Lett.* **27** 1418
[14] Roke S, Kleyn A W and Bonn M 2003 *Chem. Phys. Lett.* **370** 227
[15] Zhou H G, Fan X L, Ma L, Zhang Q H, Cui L, Zhou S M, Gui Y S, Hu C M and Xue D S 2016 *Phys. Rev. B* **94** 134421
[16] Schirhagl R, Chang K, Loretz M and Degen C L 2014 *Annu. Rev. Phys. Chem.* **65** 83
[17] Fischer M C, Madison K W, Niu Q and Raizen M G 1998 *Phys. Rev. A* **58** R2648
[18] Batalov A, Zierl C, Gaebel T, Neumann P, Chan I Y, Balasubramanian G, Hemmer P R, Jelezko F and Wrachtrup J 2008 *Phys. Rev. Lett.* **100** 077401
[19] Akhtar M N, Yousaf M, Khan S N, Nazir M S, Ahmad M and Khan M A 2017 *Ceram. Int.* **43** 17032
[20] Lin M, Duane M H and Afsar M N 2006 *IEEE Trans. Magn.* **42** 2885
[21] Rondin L, Tetienne J P, Rohart S, Thiaville A, Hingant T, Spinicelli P, Roch J F and Jacques V 2013 *Nat. Commun.* **4** 2279
[22] Horsley A, Appel P, Wolters J, Achard J, Tallaire A, Maletinsky P and Treutlein P 2018 *Phys. Rev. Appl.* **10** 044039